

Manuscript: “An optimized purification protocol for enzymatically synthesized S-adenosyl-L-methionine (SAM) for applications in solution state infrared spectroscopic studies”

Isaiah O. Odeyemi<sup>a</sup>, Teri A. Douglas<sup>a</sup>, Nosakhare F. Igie<sup>a</sup>, James A. Hargrove<sup>a</sup>, Grace Hamilton<sup>a</sup>, Brianna B. Bradley<sup>a</sup>, Cathy Thai<sup>a</sup>, Brendan Le<sup>a</sup>, Maitri Unjia<sup>a</sup>, Dylan Wicherts<sup>a</sup>, Zackery Ferneyhough<sup>a</sup>, Anjali Pillai<sup>a</sup>, Shailendra Koirala<sup>a</sup>, Laurel M. Hagge<sup>a</sup>, Raymond C. Trievel<sup>b</sup>, Robert J. Fick<sup>\*a</sup>, Allison L. Stelling<sup>\*a</sup>

a. The University of Texas at Dallas, 800W Campbell Rd., Richardson, TX, 75080, U.S.A.

b. University of Michigan, 1150 W. Medical Center Dr., Ann Arbor, MI 48109, U.S.A.

KEYWORDS: S-adenosyl-L-methionine, L-methionine, ATP, trans-methylation, L-methionine adenosyl transferase, conformational dynamics, solution state infrared spectroscopy

Corresponding authors' Email: [stelling@utdallas.edu](mailto:stelling@utdallas.edu); [Robert.fick@utdallas.edu](mailto:Robert.fick@utdallas.edu)

Corresponding authors' address: Department of Chemistry and Biochemistry, The University of Texas at Dallas, 800 W. Campbell Road, Richardson, Texas 75080, United States.

**ABSTRACT:** S-adenosyl-L-methionine (SAM) is an abundant biomolecule used by methyltransferases to regulate a wide range of essential cellular processes such as gene expression, cell signaling, protein functions, etc. Despite considerable effort, there remain many specificity challenges associated with designing small molecule inhibitors for methyltransferases, most of which exhibit off-target effects. Interestingly, NMR evidence suggests that SAM undergoes conformeric exchange between several states when free in solution. Infrared spectroscopy can detect different conformers of molecules if present in appreciable populations. When SAM is noncovalently bound within enzyme active sites, the nature, and the number of different conformations of the molecule are likely to be altered from when it is free in buffer solution. If there are unique structures or different numbers of conformers between different methyltransferase active sites, this solution-state information may provide promising structural leads to increase inhibitor specificity for a particular methyltransferase. To do this, frequencies measured in SAM's infrared spectra must be assigned to the motions of specific atoms via isotope incorporation at discrete positions. The incorporation of isotopes into SAM's structure

can be accomplished via an established enzymatic synthesis using isotopically labeled precursors. However, published protocols produced an intense and highly variable IR signal which overlapped with many of the signals from SAM rendering comparison between isotopes quite challenging. We found this intense absorption to be from co-purifying salts and the SAM counterion, producing a strong, broad signal at  $\sim 1100\text{ cm}^{-1}$ . Here, we report a revised purification protocol and present the first IR spectra of isotopically labeled  $\text{CD}_3\text{SAM}$ . These results provide a foundation for isotope labeling experiments that will define which of SAM's atoms participate in individual molecular vibrations, as a means to detect specific molecular conformations.

## 1.0 INTRODUCTION

S-adenosyl-L-methionine (SAM, also known as AdoMet) is an essential sulfonium molecule found in all living organisms<sup>1-6</sup> and plays an indispensable role in numerous biochemical processes<sup>7-12</sup>. SAM's biosynthesis occurs in the cytoplasm of microbial cells or tissues of organisms, particularly in the liver<sup>13-17</sup>, through the reaction between L-Methionine and ATP in the presence of methionine adenosyl transferase (MAT), also known as SAM synthetase<sup>18,19</sup>. SAM is an important biological molecule, as it is the second most common substrate used in various biochemical reactions after adenosine-triphosphate (ATP)<sup>20,21</sup>. The molecular structure of SAM (**Figure 1**) was first described by G. L. Cantoni, in 1952, who showed how the positively charged sulfur atom's high energy activates the carbon atoms adjacent to it, making them susceptible to nucleophilic attack<sup>22,23</sup>.

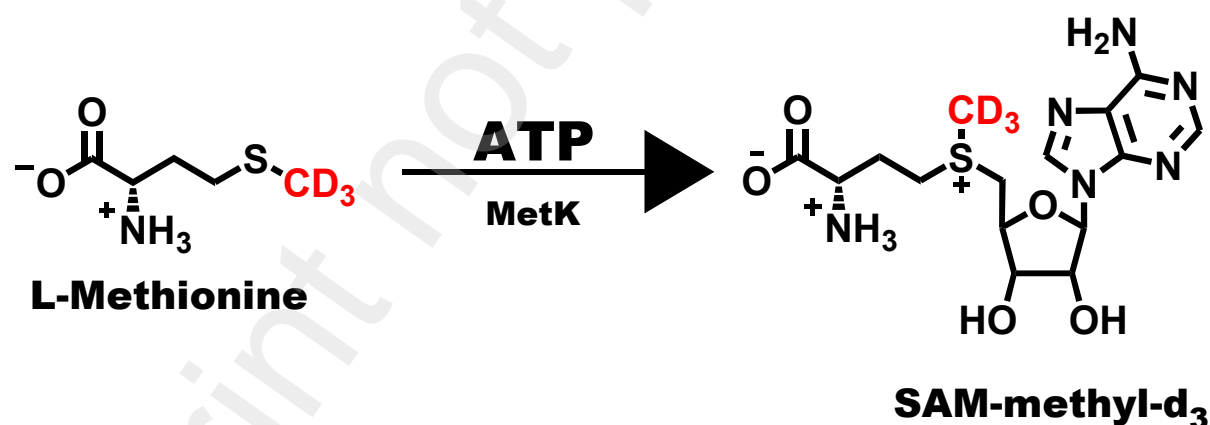


**Figure 1:** Enzymatic synthesis of SAM-methyl-d<sub>3</sub> from L-methionine-d<sub>3</sub> and ATP is catalyzed by MetK.

SAM is commonly used as the biological methyl donor by protein methyltransferases, a class of important drug targets, to regulate a wide range of essential cellular processes via methylation of different amino acids, such as lysine and arginine residues<sup>24-33</sup>. Dysregulation of several protein methyltransferases have been implicated in disease, particularly cancer, rendering them attractive

targets for drug design<sup>34–38</sup>. However, designing small molecule inhibitors that target specific protein methyltransferases has remained challenging due to selectivity issues resulting in off-target effects in this large class of enzymes, and few compounds have made it to human trials and been approved by the FDA<sup>27,39–44</sup>. SAM is a conformationally flexible molecule and can adopt numerous conformations, as observed in crystal structures of different classes of SAM-dependent methyltransferases<sup>45</sup>. Additionally, NMR data indicates that SAM is multi-conformeric when free in solution and the molecule can adopt multiple energetically reasonable physical conformations when bound with methyltransferase active sites, underscoring its conformational dynamics<sup>46–52</sup>.

Knowledge of the number of energetically permitted conformers and their spatial arrangements for the small molecule present in the solution is crucial to understanding any specific conformational poises that it can adopt within the active site of a given methyltransferase<sup>53–55</sup>. To gain insights into the number of available conformations present under a given set of conditions, solution-state structural studies are required to characterize SAM's molecular structure when free, and when bound to methyltransferases<sup>56–61</sup>. Although NMR spectroscopy has been widely used to investigate SAM dynamics, the timescales of NMR experiments may mask SAM conformations that are in rapid exchange. In contrast, vibrational spectroscopy offers exquisite sensitivity in detecting molecular conformations undergoing rapid exchange and is ideally suited for characterizing the conformational dynamics of SAM<sup>59,60,62,63</sup>. Structural knowledge gained from these studies can be leveraged in designing inhibitors that more effectively compete with the different molecular conformations that SAM adopts within a methyltransferase active site<sup>64–67</sup>.

Here, we report a revised protocol for SAM's purification that eliminates excess salts that interfere with conformer detection using vibrational spectroscopy<sup>68–71</sup>. Using the highly purified SAM, we present the first IR spectra of isotopically labeled SAM-methyl-d<sub>3</sub>. These results will provide a foundation for performing rigorous isotope studies to assign the vibrational transitions observed in the molecule's IR detection of any conformational states present when free in solution. Finally, these studies will pave the way for detecting and characterizing which specific conformations SAM adopts when bound, and the non-covalent interactions it forms with active site residues in methyltransferases.

## **2.0 Materials & Methods**

### *2.1 Materials*

All chemicals used in this work were reagent grade. L-Methionine-(methyl-d<sub>3</sub>) was purchased from Aldrich. Adenosine-5'-triphosphate (ATP) and N-[Tris-(hydroxymethyl)methyl]-glycine (Tricine) were purchased from Sigma-Aldrich. Isopropyl-β-D-1-thiogalactopyranoside (IPTG) was purchased from Fisher-Bioreagents. NaH<sub>2</sub>PO<sub>4</sub>, Na<sub>2</sub>HPO<sub>4</sub>, 2-Mercaptoethanol 99% (βME), NH<sub>4</sub>OH (28-30% solution in water), and L-methionine (98%) were purchased from Acros Organics. Glacial acetic acid and hydrochloric acid were purchased from Fisher Chemicals. Tris-base was purchased from Fisher Bioreagents. *E. coli* BL21 (DE3) chemically competent cells were purchased from Invitrogen. Lysozyme (egg-white) was purchased from Alfa Aesa. Nickel-nitrilotriacetic acid (Ni-NTA) resin (50% slurry in 20% ethanol) was purchased from G-Biosciences. CM Sepharose and CG50 weak cation-exchange resins were purchased from Sigma-Aldrich. Bio-Gel P-2 media (extra fine, <45μm wet) was purchased from Bio-Rad. QAE Sephadex A-25 was purchased from Cytiva. The plasmid which encodes S-adenosyl-methionine synthetase (*MetK*) was donated by Dr. Dewey McCafferty at Duke University.

## 2.2 Analytical Methods and Instruments

### 2.2.1 Preparation of QAE Carbonate Slurry

QAE Sephadex resin was hydrated in 1M NaCl and kept at room temperature overnight. 80 mL of hydrated QAE chloride was transferred into a 100 mL column (to account for swelling in the water wash) and equilibrated with 8-column volumes of 800 mM sodium carbonate solution, followed by washing with 20-column volumes of water. QAE carbonate was stored at room temperature.

### 2.2.2 Expression and purification of SAM synthetase (*MetK* or *MetX*)

The enzymatic synthesis of S-adenosyl-L-methionine (AdoMet) was catalyzed by *MetK* from *E. coli* using L-methionine and ATP<sup>2272,73</sup>. *MetK* was overexpressed in *E. coli* and purified as previously published,<sup>72,74</sup> and the SDS PAGE gel image of purified *MetK* is shown in **Figure S1**. The *MetK* enzyme migrates at 43 kDa, which is consistent with the sequence published by George D. Markham<sup>72</sup>. The concentration of enzyme and SAM were routinely monitored, during and after production, using a Nanodrop One-c UV-visible spectrometer from Thermo-Scientific<sup>75</sup>. Incubation of cell media for protein expression was done using the incu-shaker from INFORS. Mechanical disruption of the *E. coli* cell wall was performed with a Qsonica sonicator<sup>76</sup>. The soluble protein was separated from cell debris using a Sorvall Lynx 6000 centrifuge from Thermo-scientific. Detailed procedure for *MetK* expression and purification is provided in the supplementary data section 1.0.

### 2.2.3 HPLC Analysis

High-performance liquid chromatography (HPLC) was performed using a Vanquish system equipped with a multi-wavelength UV detection from Thermo-Scientific. The HPLC is equipped with an autosampler, which expedites the analysis of multiple samples. HPLC analyses were carried out with a HILIC XBridge Amide column (4.6 mm x 150mm, 3.5  $\mu$ m), using acetonitrile and sodium citrate buffer (10 mM, pH 3.0 mM with 25 mM NaCl). The column compartment temperature (40°C), pump (1.00 mL/min), and the system were allowed to stabilize for about 20 minutes while the baseline is monitored. The sample was run with a 4-minute gradient of 20% to 50% citrate buffer, followed by 4 minutes of 50:50%. The column was then re-equilibrated to 80:20 acetonitrile: citrate buffer for 7 minutes before the next sample. Methyl-thioadenosine (MTA), adenosine, S-adenosyl-L-homocysteine (SAH), and S-Adenosyl-L-methionine chloride (SAM) eluted at 2.1, 3.1, 5.3, and 5.9 minutes respectively. HPLC data processing was performed using Chromeleon software.

#### 2.2.4 IR analysis

The IR spectra were measured using a PerkinElmer FTIR spectrometer Spectrum 3, equipped with a Pike Technologies MIRacle Universal Attenuated Total Reflectance (ATR). IR measurements were taken at room temperature with 128 scans, 4  $\text{cm}^{-1}$  resolution, using ultrapure water as the background. The background spectrum was subtracted from the sample spectrum by the auto background-removal function on the IR spectrometer. 6  $\mu$ L of ultrapure water was first run as background, followed by 6  $\mu$ L of the sample. To prevent sample evaporation, a 25  $\mu$ L Teflon cap from PIKE technology may be used to cover samples during analysis. PerkinElmer Spectrum software was used to process infrared data. Before normalization, a multipoint baseline was added using the interactive baselining function. After baseline and normalization of the IR spectra, the difference function was used to perform spectra subtraction to see the difference between the spectra.

#### 2.2.5 NMR analysis

Nuclear magnetic resonance (NMR) experiments were conducted using a Bruker Avance III 600-MHz instrument. The sample was prepared for analysis by several rounds of lyophilization and resuspension in  $\text{D}_2\text{O}$ . The acquired data were analyzed using Topspin software from Bruker.

#### 2.2.6 Mass spectroscopic analysis

Liquid chromatography-mass spectroscopy (LC-MS) was conducted using an Agilent 1100 HPLC with a C-18 column for separation and an AB Sciex 4000 QTRAP system for mass detection. The sample was prepared in a 1:1 acetonitrile/water solution and run on LC for 30 minutes with gradient elution from 10-90% acetonitrile in  $\text{H}_2\text{O}$  (both 0.1% TFA).

#### 2.2.7 SAM Synthesis and Purification

A typical 50 mL reaction consisted of the following reagents: 200 mM Tricine/HCl pH 8.7, 50 mM KCl, 30 mM MgCl<sub>2</sub>, 8% v/v βME, 15 mM ATP, 10 mM L-Methionine, and 75 mg of MetK. The reaction was placed on a shaker (95 rpm) at room temperature. SAM production was monitored using HPLC analysis at time points from 5 mins to 240 minutes. Optimal SAM production with minimal SAH formation was observed at about 2 hours 30 mins, but for higher SAM yield the reaction was extended to about 3 hours 30 minutes. Once the reaction is completed, the mixture was spun at 4000 xg for 10 minutes to remove the precipitated enzyme. The supernatant was decanted and filtered through a 0.8 μm syringe filter. A 10 mL CG50 column was equilibrated with 15 column volumes (CV) of 1 M ammonium acetate buffer (pH 5.0), followed by 10 CV of ultrapure water. The filtrate was then loaded onto the column using the sample pump, followed by washing with 30 CV of water to remove the nonbinding components of the reaction mixture. SAM was eluted with a 20 CV gradient of water to 100 mM hydrochloric acid followed by 10 CV of hydrochloric acid. The purity of the fractions was determined by HPLC, and clean fractions were pooled and neutralized by titrating with QAE-carbonate slurry in water to pH 6.5. The neutralized solution was filtered through a 0.8 μm sterile syringe filter to remove the QAE Sephadex resin. The filtrate was then concentrated by rotary evaporation and loaded on a 25 mL Biogel-P2 column which was equilibrated with 10 mM HCl or water. After sample injection from a 250 μL sample loop, 2.5 CV of 10 mM HCl or ultrapure water was used to elute SAM, followed by column wash using 2.5 CV of ultrapure water if HCl was used. Fractions were analyzed using the HPLC method as described in **section 2.2.3** to determine the purity of the fractions. Fractions with pure SAM were pooled if they had a conductivity < 3 mS/cm and concentrated using a rotary evaporator. **Figure 2** shows the schematic representation of the enzymatic synthesis and purification SAM. Ion-exchange chromatography and size-exclusion chromatography were conducted at 4°C using medium-pressure Next-Generation Chromatography (NGC) from Bio-Rad laboratories <sup>77</sup>.

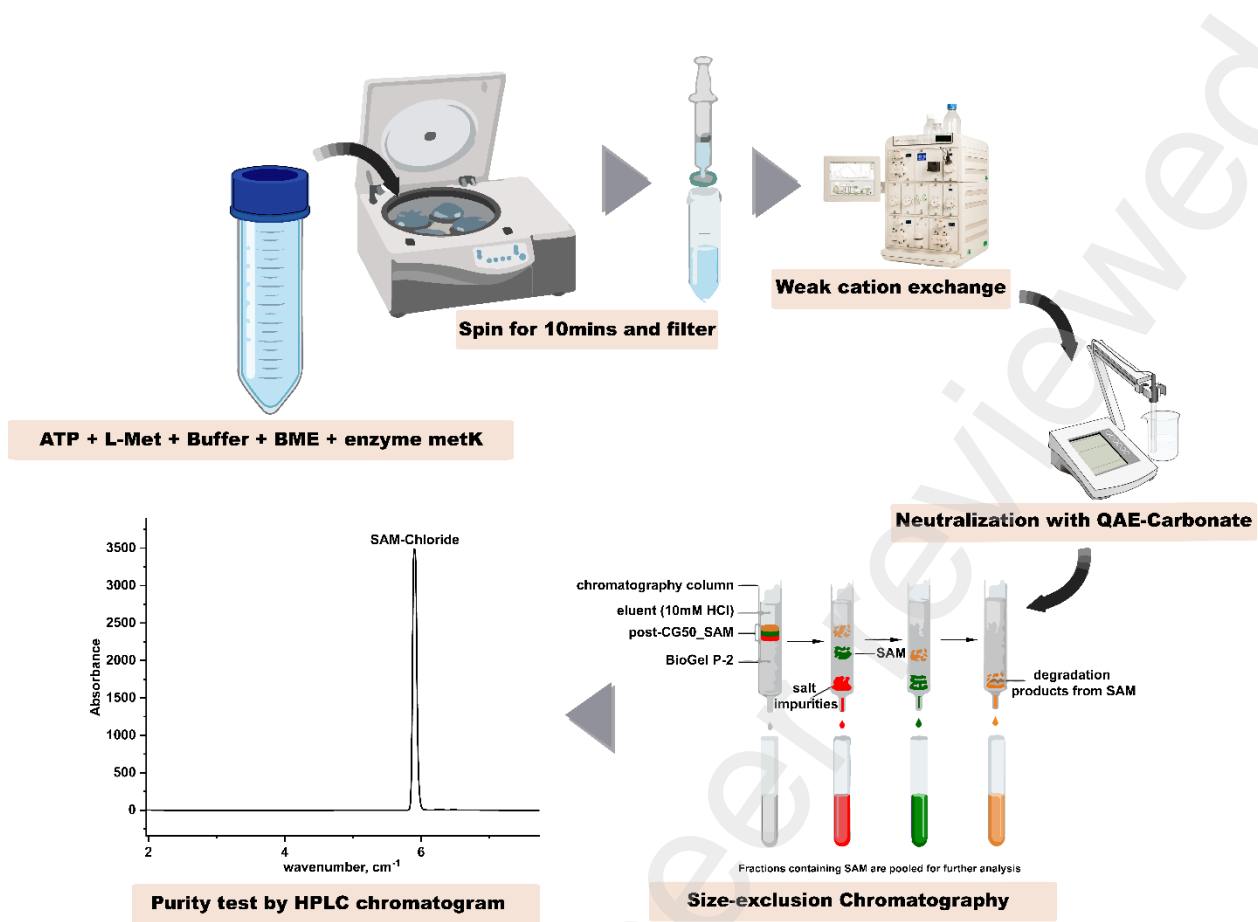


**Figure 2:** Flowchart shows the optimized method for the synthesis and purification of SAM for infrared spectroscopic studies.

### 3.0 Results and Discussion

#### Results

The major challenge faced with the determination of the IR spectrum of SAM (obtained using the previously published protocol) in liquid water is the presence of a strong signal from the polyatomic counterion, which produces a strong absorption at  $\sim 1100\text{ cm}^{-1}$  that is likely due to S=O stretching of the sulfate ion. The observed sulfate ion came from the sulfuric acid which was used to elute SAM from the ion exchange column in the existing protocol and co-purified with SAM as a counterion and as  $\text{Na}_2\text{SO}_4$  salt<sup>78</sup>. This strong signal hinders the detection of the weaker signals from SAM's ground state vibrational transitions in a spectral region where C-H vibrations are expected to be observed (specifically, transitions from bending motions of the C-H bonds), as seen in **Figure 3**. Also, since it is difficult to determine the specific concentration of salt produced alongside SAM during purification, the subtraction done to remove the IR signal of liquid water by using buffer as a "blank" during the background scans resulted in batch-to-batch inconsistencies, and obtaining replicate spectra was quite challenging. Therefore, we sought to modify the conditions of original purification to eliminate the strong sulfate signal that overlaps with several SAM signals important for confirmation of isotope incorporation. For example, the C-H bending modes that are expected to be impacted by deuteration at the reactive methyl group cannot be observed in **Figure 3**, due to the much more intense signal from the sulfates.

The SAM enzymatic synthesis is composed of two major steps: SAM production from an  $\text{S}_{\text{N}}2$  reaction between the methionine and adenosine moiety of ATP, followed by the second step which involves the hydrolysis of triphosphate to form pyrophosphate and orthophosphate, which happens before SAM is released from the enzyme<sup>79</sup> (**Figure 1**: SAM reaction).

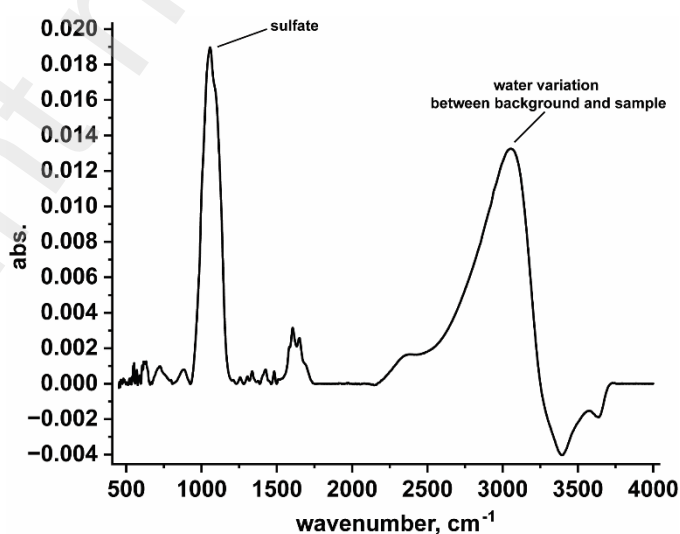


**Figure 3:** IR spectrum of SAM shows the intense sulfate peak at  $\sim 1100\text{ cm}^{-1}$  that overlaps with the SAM vibrational signals and the poor background subtraction of the water “blank” due to high salt concentration ( $\sim 3000\text{ cm}^{-1}$ ). The absorption of the salt peak is 6-fold higher than the SAM’s carbonyl signal and varies batch-to-batch.

The existing protocol was altered in the following ways. The reaction buffer for the SAM reaction was changed to tricine, compared to the previous protocol in which Tris was used. This change is made because Tris can form a cationic species that binds alongside SAM to the weak cation exchange column at neutral pH. On the other hand, Tricine forms a zwitterion at physiological pH. Since both Tris and Tricine have similar pKa values, tricine is a better buffer option due to its zwitterionic property<sup>80,81</sup>. The concentration and pH of the reaction buffer were also changed to 200 mM pH 8.7 contrary to 100 mM pH 8.0, used in the previous methods<sup>68,82</sup>. This change was introduced because as ATP is converted to SAM, acid is produced from the hydrolysis of the phosphoric acid anhydride bond, lowering the pH of the reaction mixture<sup>83,84</sup>. Metk has an isoelectric point (pI) of 5.38 and becomes less soluble as the reaction pH approaches this value. To increase enzyme stability, both the concentration of the buffer reagents and the pH of the buffer were increased.

The enzymatic synthesis was allowed to progress for  $\sim 3$  hours and 30 minutes at room temperature and purified, first with weak-cation exchange which removes the anions and neutral impurities such as methyl-thioadenosine (MTA), S-adenosyl-homocysteine (SAH), Adenosine, and ATP. SAM and the cationic impurities in the reaction bind to the column and were eluted with a hydrochloric acid gradient (**Figure 4A**). The weak cation exchange resin CM-52, a cellulose-based resin that was utilized in previous protocols<sup>85</sup> is no longer commercially available. CM-52 was replaced with CM-Sephadex, then with CG50, a methacrylic-based resin with a carboxylic functional group. CG50 was used in this study because it gave a higher yield when compared with CM-Sephadex. SAM was eluted from the CG50 using 100 mM HCl in place of sulfuric acid in the previous protocols. Conductivity increases across the curve with increasing HCl which protonates the carboxylate groups on the CG50 column, releasing SAM (**Figure 4A**). As noted, SAM and the sulfate ion spectra sum with each other, making detection of the SAM signals difficult under the strong sulfate signal. This problem was resolved by replacing the polyatomic sulfate counterion with the monatomic chloride counterion. In addition, the equilibration buffer was switched from sodium acetate, which was used in the previous protocols, to ammonium acetate for equilibration of the cation exchange column, with the goal of removing the resulting ammonium chloride by lyophilization. However, the ammonium chloride salt was not adequately removed due to its low vapor pressure of ammonium chloride at room temperature, and heating the sample would lead to SAM degradation<sup>86–88</sup>. However, ammonium chloride was observed to separate better from SAM than sodium chloride salt, allowing us to separate excess salt from SAM using the Biogel-P2 size exclusion column (**Figure 4B**). SAM elutes at a pH value of 1.5. To study SAM at a neutral pH, the previously established methods in the literature used QAE-hydroxide to neutralize the pooled fractions. QAE Sephadex A-25 is a strong anion exchange resin, purchased as

QAE-chloride, and can be readily exchanged to a preferred counterion by washing with a high-concentration solution. QAE-hydroxide was prepared by washing QAE-chloride with sodium hydroxide. However, zero conductivity was not attained during the subsequent water wash in the preparation of QAE-hydroxide resin, indicating that there was residual sodium hydroxide within the resin. To circumvent this issue, the QAE-hydroxide resin was replaced with QAE-carbonate resin which was prepared by washing QAE-chloride with 800mM sodium carbonate. Zero conductivity was attained upon washing with ultra-pure water suggesting a lack of contaminating sodium species. QAE-carbonate was used to neutralize SAM to a pH value of 6.5 and any ammonium carbonate formed during the neutralization decomposed in the vacuum during concentration using a rotatory evaporator or separated in the next column.

The next step involves desalting the SAM using Biogel-P2, a size exclusion resin, and eluting with 10 mM HCl or ultrapure water. Desalting was achieved by pooling fractions with the lowest to no conductivity (less than 3.0 mS/cm). Fresh Biogel-P2 resin was used for each purification to prevent transferring impurities to subsequent purifications. We observed that Biogel-P2 appears to have an intrinsic affinity for SAM and contaminants, at low ionic strength eluting past one column volume **Figure 4B**. A chromatography system equipped with UV and conductivity detectors allowed us to assess SAM concentration and ionic strength when pooling fractions. This minimizes ionic contamination after the final column. **Table S1** shows a summary of all the changes made to the previous protocol to obtain SAM adequate for IR studies.

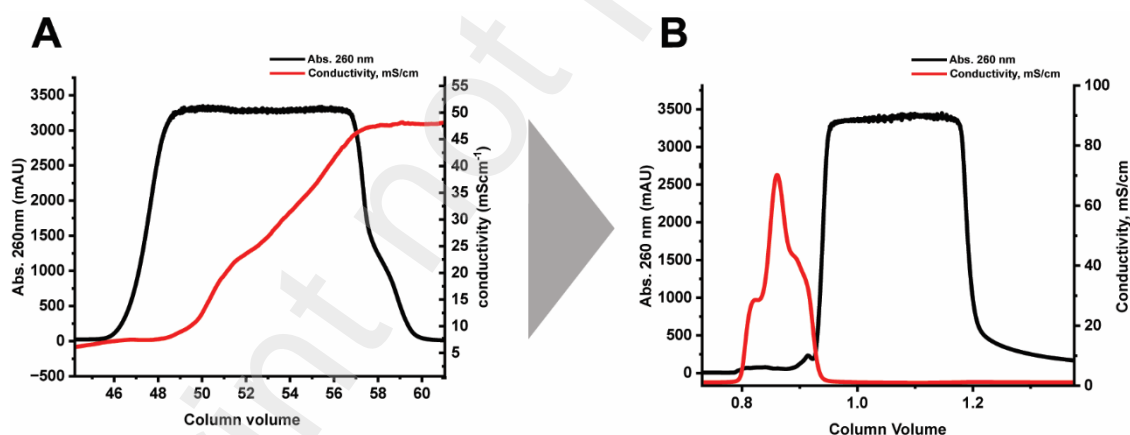


**Figure 4:** (A) The CG50 weak cation exchange column was equilibrated with 1M ammonium acetate (pH 5.0), followed by linear gradient elution with 100 mM HCl. The black trace is the absorbance at 260 nm and the red trace shows conductivity as it increases across the plot. (B) Desalting of SAM using the Biogel-P2 column. SAM is observed to have some affinity with the column as salt elutes earlier and SAM elutes after one column volume.

## HPLC

HPLC analysis was conducted to verify the purity of the SAM fractions after each column before pooling them. Fractions containing SAM from the first purification step were analyzed by HPLC as described earlier in **Section 2.2.3** to confirm the absence of adenine-containing impurities. **Figure 5** shows the 260 nm absorbance trace of impure, commercial, and clean SAM.

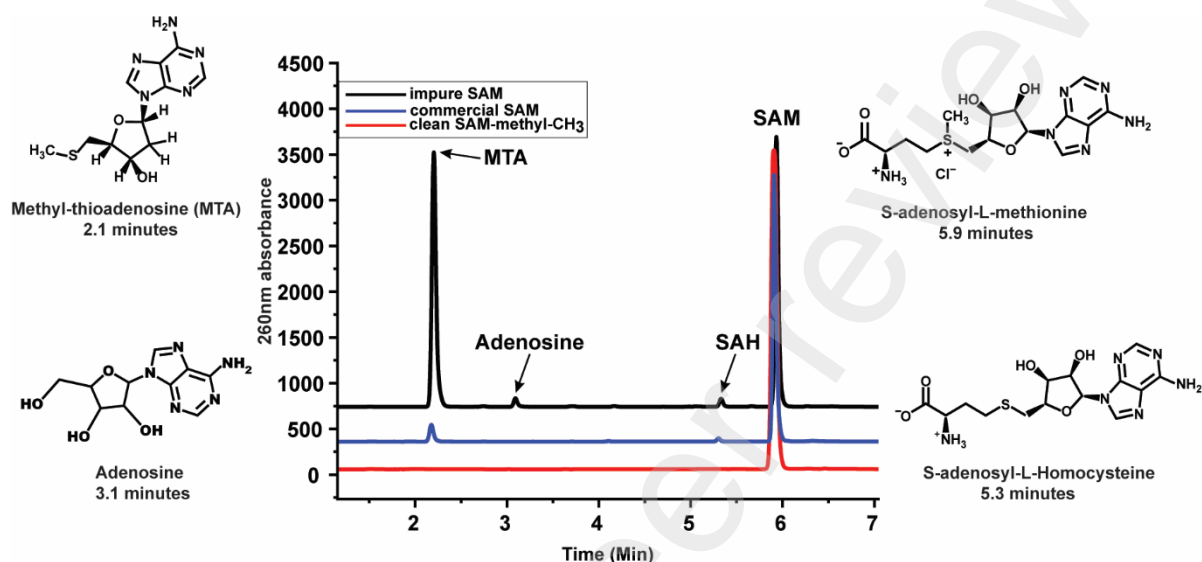


**Figure 5:** The **black** trace was obtained from impure fractions of SAM that were deliberately taken for HPLC analysis during SAM purification. The fraction was found to contain impurities such as Adenosine, SAH, and MTA. The absorbance trace shown in **blue** was the commercial SAM and was found to contain MTA and SAH as impurities. The absorbance trace shown in **red** was the clean SAM synthesized and purified in our lab which contains none of the impurities found in both the impure and the commercial SAM.

## Proton NMR

Proton NMR analysis was conducted as discussed in **section 2.2.5**. As expected, the  $^1\text{H-NMR}$  did not show any difference between SAM with low or high conductivity. **Figure 6** shows the  $^1\text{H-NMR}$  spectrum of pure SAM-methyl- $\text{CH}_3$  (low conductivity). The pure SAM-methyl- $\text{CH}_3$  was overlaid with high conductivity-SAM (high conductivity fractions of SAM) to ascertain whether there are any differences in their spectra. No significant difference was observed. SAM has two chiral centers which result in four possible stereoisomers. The sulfonium chiral center can racemize to form (S)- and (R)-epimers, which are optically stable and can be separated. However, only the (S)-epimer is the only biologically active form of SAM. The (S)-epimer is observed as a singlet peak, 3H of the methyl- $\text{CH}_3$  at 2.92 ppm, and the (R)-epimer at 2.88 ppm (**Figure 6**). Matos and Wong studied the stability and stabilization of SAM and reported the major factors that affect the stability and epimerization of the (S)-epimer to (R)-epimer of SAM are the pH, temperature, and sulfonium counterion <sup>89</sup>. Mark L. et al., studied the stereochemistry of SAM in  $\text{D}_2\text{O}$  using NMR by measuring the coupling constants between the protons on the chiral centers <sup>90</sup>. There have also been several NMR studies of the conformational dynamics of SAM in solution <sup>49</sup>.

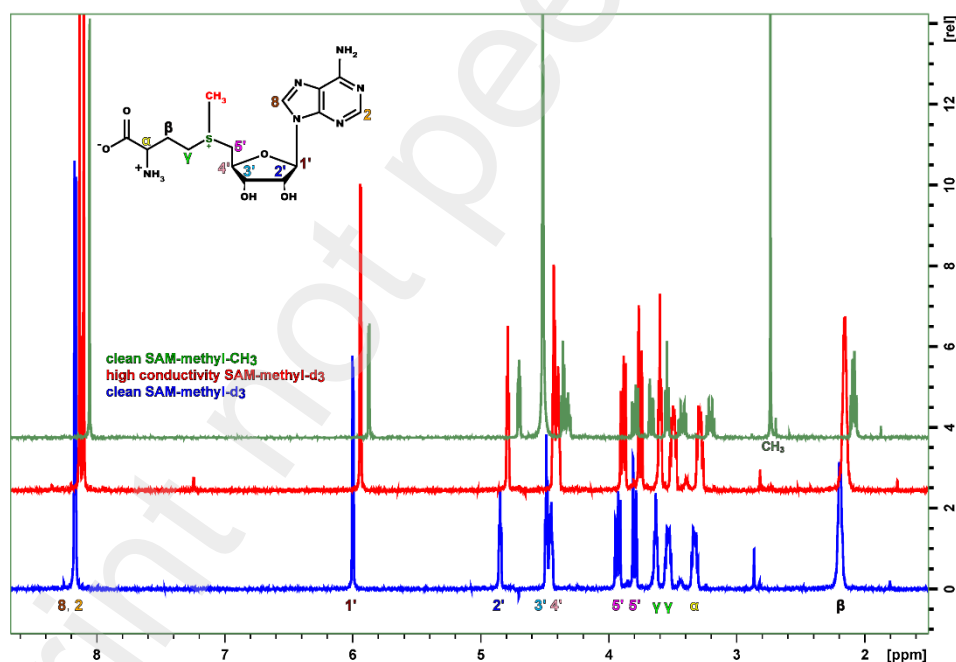


**Figure 6:** Overlay of the NMR spectra of SAM-methyl- $\text{CH}_3$  (Green) and SAM-methyl- $\text{d}_3$  (Blue) with SAM fractions with high conductivity (Red).  $^1\text{H-NMR}$  ( $\text{D}_2\text{O}$ , 298 K)  $\delta$  2.26 (q, 2H, H $\beta$ ); 2.92 (s, 3H,  $\text{CH}_3$ ); 3.73 (m, 1H, H $\alpha$ ); 3.62 (m, 2H, H $\gamma$ ); 3.85, 3.98 (m, 2H, H5', 5''); 4.54 (m, 1H, H4'); 4.56 (t, 1H, H3'); 4.89 (t, 1H, H2'); 6.07 (d, 1H, H1'); 8.25 (s, 1H, H2); 8.25 (s, 1H, H8)

## ESI-MS

**Figure 7A** shows the  $m/z$  of non-labeled SAM-chloride with  $m/z$   $M^+$  calculated for  $C_{15}H_{23}N_6O_2S^+$  of 399.15 and found as 399.2 correspond with the purchased non-labeled SAM (**Figure 7B**). As expected, fractions with high conductivity also show SAM with similar  $m/z$  399.36 in **Figure 7D**. Isotopically labeled SAM-chloride is shown to have an  $m/z$  calculated for  $C_{15}D_3H_{20}N_6O_2S^+$  of 402.16 and found as 402.32 (**Figure 7C**). A column blank was obtained by blank injection into the mass spectrometer **Figure S2**.

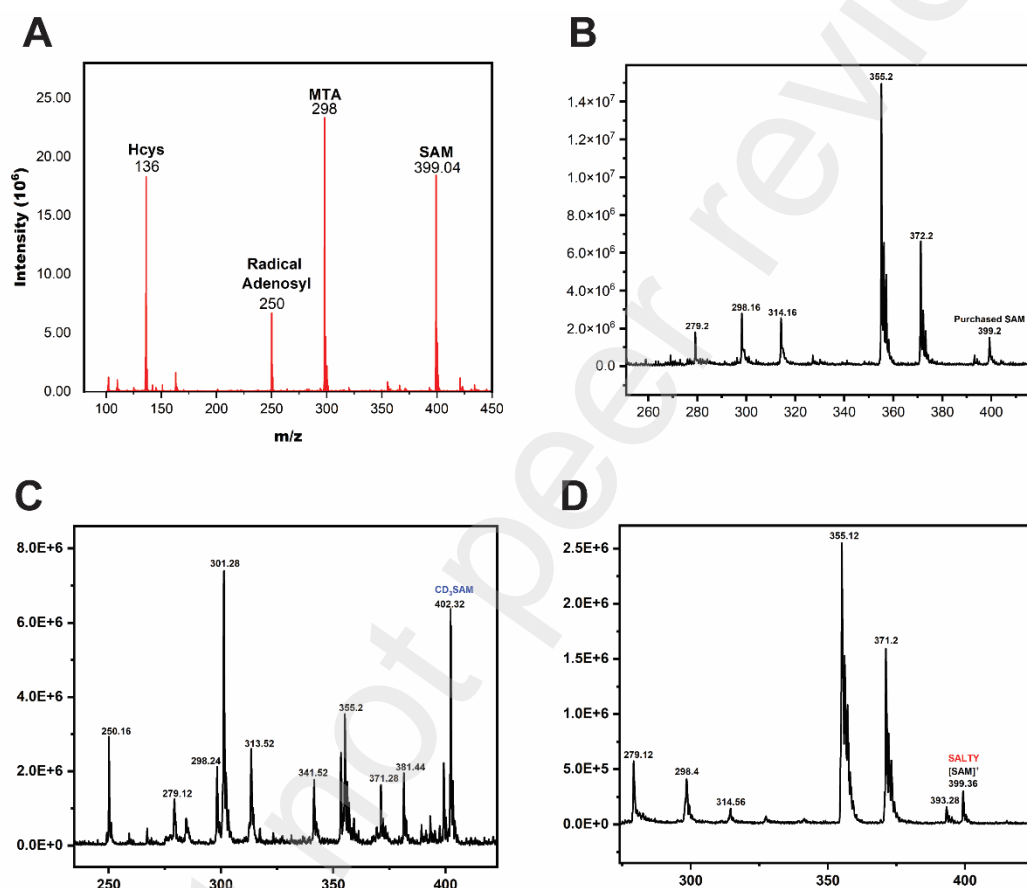


**Figure 7:** (A) Non-labeled SAM  $m/z$   $M^+$  calculated for  $C_{15}H_{23}N_6O_2S^+$  399.15; observed 399.2 (B) Commercial SAM, calculated for  $C_{15}H_{23}N_6O_2S^+$  399.15; observed 399.2 (C) SAM-methyl-d<sub>3</sub>: calculated for  $C_{15}D_3H_{20}N_6O_2S^+$  402.16; found 402.32 (D) High conductivity-SAM, calculated for  $C_{15}H_{23}N_6O_2S^+$  399.15; observed 399.36.

## IR analysis

The IR spectra of SAM indicated there was excess salt present in the mixture after the final purification column, resulting in a strong IR signal at  $\sim 1100\text{ cm}^{-1}$  that likely arises from the S=O stretching of the counterion and the excess sodium sulfate salt. Previous protocols elute SAM with sulfuric acid and produce sulfate counterions<sup>91,92</sup>. **Figure 8A** shows the IR spectrum of the final mixture containing both SAM and the sulfate counterion. Evidence for the signal being due to molecular vibrations from the sulfate ion and not SAM is evident as the interfering signal exhibits a large shift in positions (from  $\sim 1100\text{ cm}^{-1}$  to  $\sim 1450\text{ cm}^{-1}$ ) when a different salt is present in the purification. Fractions with high conductivity from the Biogel P2 column possess an intense ammonium peak at  $1450\text{ cm}^{-1}$  region<sup>93-95</sup> (**Figure 8B**). However, fractions containing low to no conductivity ( $<3.0\text{ mS/cm}$ ) lack salt impurities/ammonium peak as seen in the black trace (**figure 8B**). Replicate, batch-to-batch (separate purifications) spectra of SAM-chloride were taken, with their mean and standard deviation plot shown in **Figure 9**.

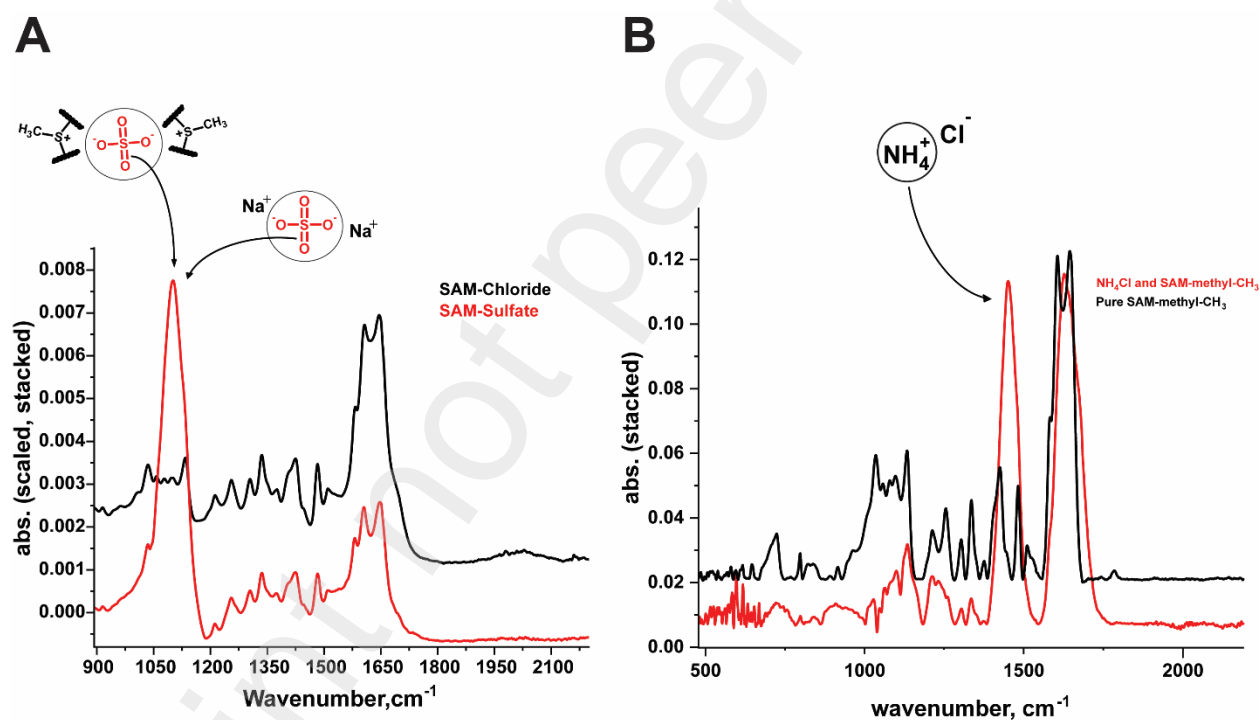


**Figure 8:** (A) Intense sulfate peak at about  $\sim 1100\text{ cm}^{-1}$  (red) hinders band assignment of the SAM IR spectrum. This analytical challenge was solved by exchanging sulfate for chloride and eluting SAM with HCl during cation exchange. (B) The intense signal at  $\sim 1450$  (red) is the ammonium from ammonium chloride which was separated from SAM using BiogelP-2 ultrafine resin. Successful desalting of SAM was achieved by pooling fractions with low ( $<3.0\text{ mS cm}^{-1}$ ) to no conductivity.

Having confirmed the reproducibility of our method with the light isotopes, SAM-(methyl-d<sub>3</sub>) was enzymatically synthesized utilizing a commercially available isotopically labeled precursor, L-Methionine-(methyl-d<sub>3</sub>), and our optimized SAM purification scheme. The synthesis of SAM-methyl-d<sub>3</sub> was confirmed using IR spectroscopy to compare the C-H and C-D stretching regions between the light and heavy isotopes of SAM. **Figure 9A** below shows the mean and standard deviation plot of two-batch replicates of SAM-methyl-d<sub>3</sub>, with the bold line as the mean and the grey-shaded region as the standard deviation. Shown in green is the noise line obtained from the SAM-methyl-d<sub>3</sub> spectra. **Figure 9B** shows the SAM-methyl-CH<sub>3</sub> IR spectrum and the noise line (shown in red) obtained by averaging the difference between the spectrum of the same batch of purified SAM. As expected, perturbation in the 1100 cm<sup>-1</sup> region of the SAM-methyl-d<sub>3</sub> spectrum is due to C-H stretching. The observed perturbations indicate the successful incorporation of the deuterated isotope. These expected perturbations are seen in the difference spectrum taken between SAM-methyl-CH<sub>3</sub> and SAM-methyl-d<sub>3</sub> **Figure 10**.

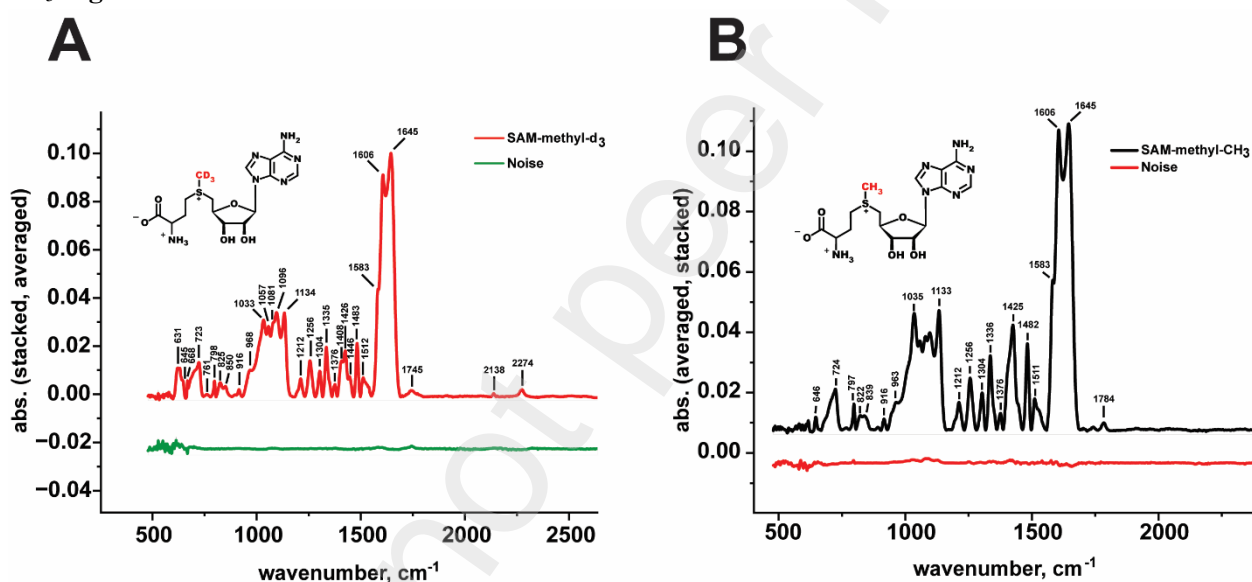


**Figure 9:** (A). SAM-methyl-d<sub>3</sub> IR spectrum shows the mean (in bold line) and standard deviation (in the grey-shaded region). In green is the noise line obtained by subtracting two different spectra of the same batch of purified SAM-methyl-d<sub>3</sub>. Perturbation in the C-H stretching region ~1100 cm<sup>-1</sup> is evidence of isotope incorporation (B) IR spectrum of SAM-methyl-CH<sub>3</sub>. The red line is the noise line obtained from the difference between two different spectra of the same batch of purified SAM-methyl-CH<sub>3</sub>.

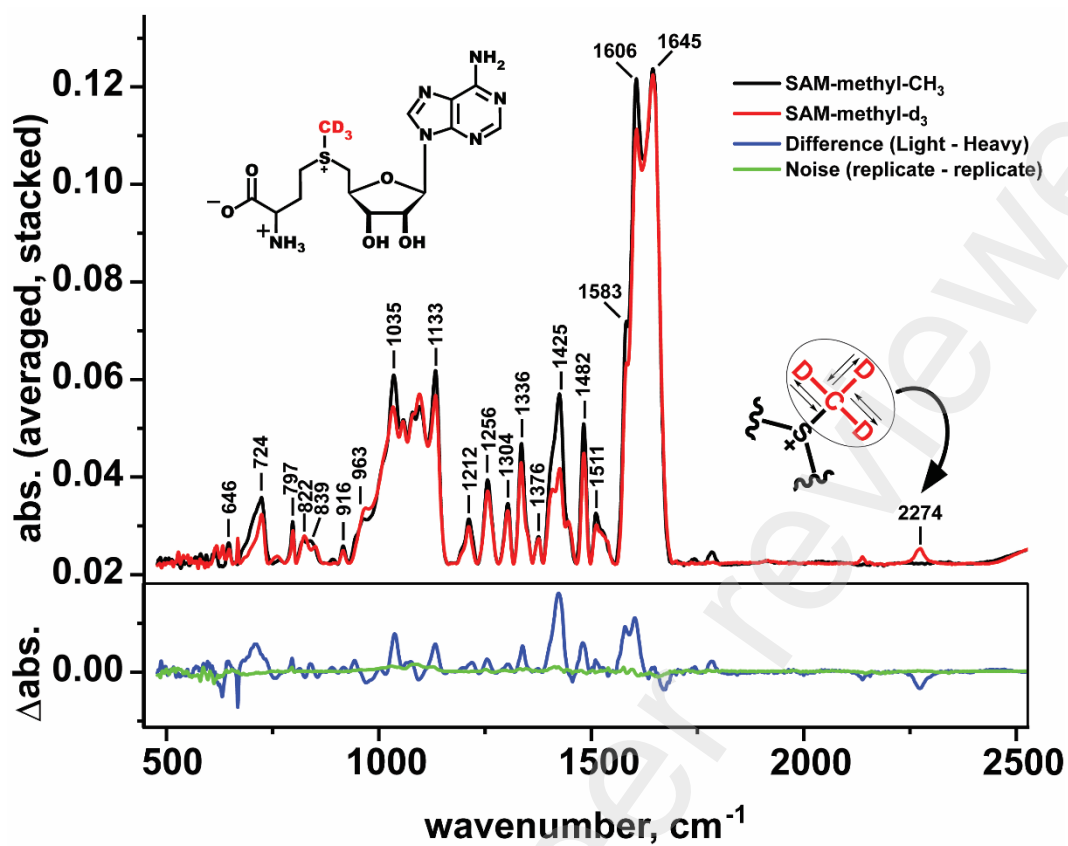


**Figure 10:** Shows the spectrum of SAM-methyl-d<sub>3</sub> (RED) and SAM-methyl-CH<sub>3</sub> (BLACK) ~100 mM. The noise line (GREEN) was obtained from the natural abundance of SAM-methyl-CH<sub>3</sub> spectra, and the difference (BLUE) was obtained by subtracting the heavy spectrum from light.

## Conclusion

The assignment of the infrared (IR) signals from S-adenosylmethionine in solution to the motions of specific atoms in its molecular structure via isotope labeling experiments has been complicated by the presence of a strong signal from the counterion resulting from its purification and salt that co-purify with SAM after its synthesis. These ions produce an IR signal far stronger than the molecule of interest (SAM), masking its signals and rendering detection of key spectral regions challenging<sup>78</sup>. The optimized purification method described here effectively removes these ionic hindrances to the detection of SAM's IR signals, which are otherwise undetectable via other methods such as NMR, mass spectroscopy, HPLC, and electron paramagnetic spectroscopy (EPR)<sup>68,74,90,96</sup> and enables the acquisition of high-quality IR spectra of naturally abundant and isotopically labeled SAM in the solution state. The spectral signal exhibits excellent signal-to-noise ratios, allowing for precise spectral analysis and assignment of transitions from specific functional group normal modes to the observed signals in SAM's experimental spectrum. Our results pave the way for assigning observed frequencies of transition in the linear IR spectrum to specific atomic motions in SAM's molecular structure via isotope labeling. Future work will seek to identify IR signals that will be faithful reporters of SAM's conformation when bound in methyltransferase active sites. These signals can also serve as molecular-scale meters to measure the enthalpies of the noncovalent interactions SAM experiences when in active site environments, which function to accelerate the rates of the myriad of SAM-dependent enzyme-catalyzed reactions<sup>97-99</sup>.

In conclusion, our study offers a robust and effective method for obtaining high-quality IR spectra of SAM in solution and lays the foundation for further investigations into the vibrational properties of this important small biomolecule.

## ASSOCIATED CONTENT

**Supporting Information.** The detailed method for protein expression and purification, MS, NMR data for SAM.

## AUTHOR INFORMATION

### Corresponding Authors

**Allison L. Stelling** - Department of Chemistry and Biochemistry, The University of Texas at Dallas, 800 W. Campbell Road, Richardson, Texas 75080, United States.

Email: [stelling@utdallas.edu](mailto:stelling@utdallas.edu)

**Robert J. Fick** - Department of Chemistry and Biochemistry, The University of Texas at Dallas, Richardson, Texas, 75080, United States

Email: [Robert.fick@utdallas.edu](mailto:Robert.fick@utdallas.edu)

### Authors' Present Addresses

**Isaiah Odeyemi** - Department of Chemistry and Biochemistry, The University of Texas at Dallas, 800 W. Campbell Road, Richardson, Texas 75080, United States; <https://orcid.org/0000-0002-8369-9130>

Email: [isaiah.odeyemi@utdallas.edu](mailto:isaiah.odeyemi@utdallas.edu)

**Teri A. Douglas** – Department of Chemistry and Biochemistry, The University of Texas at Dallas, Richardson, Texas, 75080, United States

**Nosakhare F. Igie** - Department of Chemistry and Biochemistry, The University of Texas at Dallas, Richardson, Texas, 75080, United States; <https://orcid.org/0000-0001-7590-0757>

**James A. Hargrove** – Current address: Department of Food Science, North Carolina State University, Raleigh, NC, United States

**Raymond Trievel** (UM) – Department of Biological Chemistry, University of Michigan, Ann Arbor, Michigan, 48109, United States.

**Grace Hamilton** – Current address: Cleveland State University, 2121 Euclid Avenue, Cleveland, OH

**Brianna B. Bradley** - Department of Chemistry and Biochemistry, The University of Texas at Dallas, Richardson, Texas, 75080, United States

**Cathy Thai** - Department of Chemistry and Biochemistry, The University of Texas at Dallas, Richardson, Texas, 75080, United States

**Brendan Le** – Current address: Department of Chemistry and Biochemistry, Texas A&M University, College Station, TX, U.S.A.

**Maitri Unjia** - Department of Chemistry and Biochemistry, The University of Texas at Dallas, Richardson, Texas, 75080, United States

**Dylan Wicherts** - Department of Chemistry and Biochemistry, The University of Texas at Dallas, Richardson, Texas, 75080, United States

**Zackery Ferneyhough** - Department of Chemistry and Biochemistry, The University of Texas at Dallas, Richardson, Texas, 75080, United States

**Anjali Pillai** – Analytical Chemist for the Product Development team at Eurofins

**Shailendra Koirala** - Department of Chemistry and Biochemistry, The University of Texas at Dallas, Richardson, Texas, 75080, United States

**Laurel M. Hagge** - Department of Chemistry and Biochemistry, The University of Texas at Dallas, Richardson, Texas, 75080, United States

**Robert J. Fick\*** - Department of Chemistry and Biochemistry, The University of Texas at Dallas, Richardson, Texas, 75080, United States

**Allison L. Stelling\*** - Department of Chemistry and Biochemistry, The University of Texas at Dallas, Richardson, Texas, 75080, United States

### **Funding Sources**

We acknowledge the National Science Foundation (NSF-CHE-2107902), the Welch Foundation (AT-2079-20210327), and the University of Texas at Dallas startup funds for their invaluable financial support, without which this research project would not have been feasible. We are indebted to the NSF and the Welch Foundation for their unwavering dedication to advancing scientific research and fostering academic excellence.

### **ACKNOWLEDGMENT**

We thank The University of Texas at Dallas for providing the research facilities that enabled us to conduct experiments and analyze our data.

### **ABBREVIATIONS**

SAM, S-adenosyl-L-methionine; SAH, S-adenosyl-L-homocysteine; ATP, adenosine-triphosphate; MAT, L-methionine adenosyl transferase; MS, mass spectroscopy; IR, infrared spectroscopy; NMR, nuclear magnetic resonance; CV, column volume

## References

- (1) Lu, S. C. S-Adenosylmethionine. *Int J Biochem Cell Biol* **2000**, *32* (4), 391–395.
- (2) Bennett, M. R.; Shepherd, S. A.; Cronin, V. A.; Micklefield, J. Recent Advances in Methyltransferase Biocatalysis. *Curr Opin Chem Biol* **2017**, *37*, 97–106.
- (3) Dalhoff, C.; Weinhold, E. S-Adenosyl-L-Methionine and Related Compounds. *Modified nucleosides: In biochemistry, biotechnology and medicine* **2008**, 223–247.
- (4) Roje, S. S-Adenosyl-L-Methionine: Beyond the Universal Methyl Group Donor. *Phytochemistry* **2006**, *67* (15), 1686–1698.
- (5) Kozbial, P. Z.; Mushegian, A. R. Natural History of S-Adenosylmethionine-Binding Proteins. *BMC Struct Biol* **2005**, *5* (1), 1–26.
- (6) Loenen, W. A. M. S-Adenosylmethionine: Jack of All Trades and Master of Everything? *Biochem Soc Trans* **2006**, *34* (2), 330–333.
- (7) Kilwake, J. W.; Umer, M. J.; Wei, Y.; Mehari, T. G.; Magwanga, R. O.; Xu, Y.; Hou, Y.; Wang, Y.; Shiraku, M. L.; Kirungu, J. N. Genome-Wide Characterization of the SAMS Gene Family in Cotton Unveils the Putative Role of GhSAMS2 in Enhancing Abiotic Stress Tolerance. *Agronomy* **2023**, *13* (2), 612.
- (8) Perlinska, A. P.; Stasiulewicz, A.; Nawrocka, E. K.; Kazimierczuk, K.; Setny, P.; Sulkowska, J. I. Restriction of S-Adenosylmethionine Conformational Freedom by Knotted Protein Binding Sites. *PLoS Comput Biol* **2020**, *16* (5), e1007904.
- (9) Copeland, R. A.; Solomon, M. E.; Richon, V. M. Protein Methyltransferases as a Target Class for Drug Discovery. *Nat Rev Drug Discov* **2009**, *8* (9), 724–732.
- (10) Ghoshal, K.; Bai, S. DNA Methyltransferases as Targets for Cancer Therapy. *Drugs Today (Barc)* **2007**, *43* (6), 395–422.
- (11) Neganova, M. E.; Klochkov, S. G.; Aleksandrova, Y. R.; Aliev, G. Histone Modifications in Epigenetic Regulation of Cancer: Perspectives and Achieved Progress. In *Seminars in Cancer Biology*; Elsevier, 2022; Vol. 83, pp 452–471.
- (12) Hamamoto, R.; Nakamura, Y. Dysregulation of Protein Methyltransferases in Human Cancer: An Emerging Target Class for Anticancer Therapy. *Cancer Sci* **2016**, *107* (4), 377–384.
- (13) Chu, J.; Qian, J.; Zhuang, Y.; Zhang, S.; Li, Y. Progress in the Research of S-Adenosyl-L-Methionine Production. *Appl Microbiol Biotechnol* **2013**, *97* (1), 41–49.
- (14) Cederbaum, A. I.; Lu, Y.; Wu, D. Role of Oxidative Stress in Alcohol-Induced Liver Injury. *Arch Toxicol* **2009**, *83*, 519–548.

- (15) Chu, J.; Qian, J.; Zhuang, Y.; Zhang, S.; Li, Y. Progress in the Research of S-Adenosyl-L-Methionine Production. *Appl Microbiol Biotechnol* **2013**, *97*, 41–49.
- (16) Mann, J. Epigenetics in Liver Disease: Involvement of Oxidative Stress. In *Liver Pathophysiology*; Elsevier, 2017; pp 199–211.
- (17) Benkovic, S. J.; Hammes-Schiffer, S. A Perspective on Enzyme Catalysis. *Science (1979)* **2003**, *301* (5637), 1196–1202.
- (18) Grillo, M. A.; Colombatto, S. S-Adenosylmethionine and Its Products. *Amino Acids* **2008**, *34* (2), 187–193.
- (19) Shafqat, N.; Muniz, J. R. C.; Pilka, E. S.; Papagrigoriou, E.; von Delft, F.; Oppermann, U.; Yue, W. W. Insight into S-Adenosylmethionine Biosynthesis from the Crystal Structures of the Human Methionine Adenosyltransferase Catalytic and Regulatory Subunits. *Biochemical Journal* **2013**, *452* (1), 27–36.
- (20) Cantoni, G. L. Biological Methylation: Selected Aspects. *Annu Rev Biochem* **1975**, *44* (1), 435–451.
- (21) Ward, L. C.; McCue, H. v; Carnell, A. J. Carboxyl Methyltransferases: Natural Functions and Potential Applications in Industrial Biotechnology. *ChemCatChem* **2021**, *13* (1), 121–128.
- (22) Cantoni, G. L. The Nature of the Active Methyl Donor Formed Enzymatically from L-Methionine and Adenosinetriphosphate<sup>1</sup>, 2. *J Am Chem Soc* **1952**, *74* (11), 2942–2943.
- (23) Coward, J. K.; Sweet, W. D. Kinetics and Mechanism of Methyl Transfer from Sulfonium Compounds to Various Nucleophiles. *J Org Chem* **1971**, *36* (16), 2337–2346.
- (24) Copeland, R. A.; Solomon, M. E.; Richon, V. M. Protein Methyltransferases as a Target Class for Drug Discovery. *Nat Rev Drug Discov* **2009**, *8* (9), 724–732.
- (25) Wagner, T.; Jung, M. New Lysine Methyltransferase Drug Targets in Cancer. *Nat Biotechnol* **2012**, *30* (7), 622–623.
- (26) Jiang, H.; Gao, Y.; Zhang, L.; Chen, D.; Gan, J.; Murchie, A. I. H. The Identification and Characterization of a Selected SAM-Dependent Methyltransferase Ribozyme That Is Present in Natural Sequences. *Nat Catal* **2021**, *4* (10), 872–881.
- (27) Mentch, S. J.; Locasale, J. W. One-carbon Metabolism and Epigenetics: Understanding the Specificity. *Ann N Y Acad Sci* **2016**, *1363* (1), 91–98.
- (28) Murn, J.; Shi, Y. The Winding Path of Protein Methylation Research: Milestones and New Frontiers. *Nat Rev Mol Cell Biol* **2017**, *18* (8), 517–527.
- (29) Wu, Z.; Connolly, J.; Biggar, K. K. Beyond Histones—the Expanding Roles of Protein Lysine Methylation. *FEBS J* **2017**, *284* (17), 2732–2744.
- (30) Blanc, R. S.; Richard, S. Arginine Methylation: The Coming of Age. *Mol Cell* **2017**, *65* (1), 8–24.
- (31) Bedford, M. T.; Richard, S. Arginine Methylation: An Emerging Regulator of Protein Function. *Mol Cell* **2005**, *18* (3), 263–272.
- (32) Guccione, E.; Richard, S. The Regulation, Functions and Clinical Relevance of Arginine Methylation. *Nat Rev Mol Cell Biol* **2019**, *20* (10), 642–657.

- (33) Bedford, M. T. Arginine Methylation at a Glance. *J Cell Sci* **2007**, *120* (24), 4243–4246.
- (34) Heerboth, S.; Lapinska, K.; Snyder, N.; Leary, M.; Rollinson, S.; Sarkar, S. Use of Epigenetic Drugs in Disease: An Overview. *Genet Epigenet* **2014**, *6*, GEG-S12270.
- (35) Albert, M.; Helin, K. Histone Methyltransferases in Cancer. In *Seminars in cell & developmental biology*; Elsevier, 2010; Vol. 21, pp 209–220.
- (36) Nimura, K.; Ura, K.; Kaneda, Y. Histone Methyltransferases: Regulation of Transcription and Contribution to Human Disease. *J Mol Med* **2010**, *88*, 1213–1220.
- (37) Husmann, D.; Gozani, O. Histone Lysine Methyltransferases in Biology and Disease. *Nat Struct Mol Biol* **2019**, *26* (10), 880–889.
- (38) Kaniskan, H. U.; Konze, K. D.; Jin, J. Selective Inhibitors of Protein Methyltransferases. *J Med Chem* **2015**, *58* (4), 1596–1629.
- (39) Dilworth, D.; Barsyte-Lovejoy, D. Targeting Protein Methylation: From Chemical Tools to Precision Medicines. *Cellular and Molecular Life Sciences* **2019**, *76*, 2967–2985.
- (40) Kaniskan, H. U.; Martini, M. L.; Jin, J. Inhibitors of Protein Methyltransferases and Demethylases. *Chem Rev* **2018**, *118* (3), 989–1068.
- (41) Zhang, J.; Zheng, Y. G. SAM/SAH Analogs as Versatile Tools for SAM-Dependent Methyltransferases. *ACS Chem Biol* **2016**, *11* (3), 583–597.
- (42) Aouadi, W.; Eydoux, C.; Coutard, B.; Martin, B.; Debart, F.; Vasseur, J. J.; Contreras, J. M.; Morice, C.; Quérat, G.; Jung, M.-L. Toward the Identification of Viral Cap-Methyltransferase Inhibitors by Fluorescence Screening Assay. *Antiviral Res* **2017**, *144*, 330–339.
- (43) Wang, M.; Xu, R.-M.; Thompson, P. R. Substrate Specificity, Processivity, and Kinetic Mechanism of Protein Arginine Methyltransferase 5. *Biochemistry* **2013**, *52* (32), 5430–5440.
- (44) Brueckner, B.; Lyko, F. DNA Methyltransferase Inhibitors: Old and New Drugs for an Epigenetic Cancer Therapy. *Trends Pharmacol Sci* **2004**, *25* (11), 551–554.
- (45) Schubert, H. L.; Blumenthal, R. M.; Cheng, X. Many Paths to Methyltransfer: A Chronicle of Convergence. *Trends Biochem Sci* **2003**, *28* (6), 329–335.
- (46) Bame, J.; Hoeck, C.; Carrington, M. J.; Butts, C. P.; Jäger, C. M.; Croft, A. K. Improved NOE Fitting for Flexible Molecules Based on Molecular Mechanics Data—a Case Study with S-Adenosylmethionine. *Physical Chemistry Chemical Physics* **2018**, *20* (11), 7523–7531.
- (47) Klee, W. A.; Mudd, S. H. The Conformation of Ribonucleosides in Solution. The Effect of Structure on the Orientation of the Base. *Biochemistry* **1967**, *6* (4), 988–998.
- (48) Markham, G. D.; Norrby, P.-O.; Bock, C. W. S-Adenosylmethionine Conformations in Solution and in Protein Complexes: Conformational Influences of the Sulfonium Group. *Biochemistry* **2002**, *41* (24), 7636–7646.
- (49) Markham, G. D.; Norrby, P.-O.; Bock, C. W. S-Adenosylmethionine Conformations in Solution and in Protein Complexes: Conformational Influences of the Sulfonium Group. *Biochemistry* **2002**, *41* (24), 7636–7646.

- (50) Chen, B.; LeBlanc, R.; Dayie, T. K. SAM-II Riboswitch Samples at Least Two Conformations in Solution in the Absence of Ligand: Implications for Recognition. *Angewandte Chemie* **2016**, *128* (8), 2774–2777.
- (51) Chen, B.; Zuo, X.; Wang, Y.-X.; Dayie, T. K. Multiple Conformations of SAM-II Riboswitch Detected with SAXS and NMR Spectroscopy. *Nucleic Acids Res* **2012**, *40* (7), 3117–3130.
- (52) Haller, A.; Rieder, U.; Aigner, M.; Blanchard, S. C.; Micura, R. Conformational Capture of the SAM-II Riboswitch. *Nat Chem Biol* **2011**, *7* (6), 393–400.
- (53) Hammes, G. G. Multiple Conformational Changes in Enzyme Catalysis. *Biochemistry* **2002**, *41* (26), 8221–8228.
- (54) James, L. C.; Tawfik, D. S. Conformational Diversity and Protein Evolution—a 60-Year-Old Hypothesis Revisited. *Trends Biochem Sci* **2003**, *28* (7), 361–368.
- (55) Benkovic, S. J.; Hammes-Schiffer, S. A Perspective on Enzyme Catalysis. *Science (1979)* **2003**, *301* (5637), 1196–1202.
- (56) Anderson, A. C. The Process of Structure-Based Drug Design. *Chem Biol* **2003**, *10* (9), 787–797.
- (57) Wang, R.; Gao, Y.; Lai, L. LigBuilder: A Multi-Purpose Program for Structure-Based Drug Design. *Molecular modeling annual* **2000**, *6*, 498–516.
- (58) Blundell, T. L. Structure-Based Drug Design. *Nature* **1996**, *384* (6604 Suppl), 23–26.
- (59) Klebe, G. Recent Developments in Structure-Based Drug Design. *J Mol Med* **2000**, *78*, 269–281.
- (60) Amzel, L. M. Structure-Based Drug Design. *Curr Opin Biotechnol* **1998**, *9* (4), 366–369.
- (61) Hu, H.; Qian, K.; Ho, M.-C.; Zheng, Y. G. Small Molecule Inhibitors of Protein Arginine Methyltransferases. *Expert Opin Investig Drugs* **2016**, *25* (3), 335–358.
- (62) Zanni, M. T.; Hochstrasser, R. M. Two-Dimensional Infrared Spectroscopy: A Promising New Method for the Time Resolution of Structures. *Curr Opin Struct Biol* **2001**, *11* (5), 516–522.
- (63) Benfield, R. E.; Braga, D.; Johnson, B. F. G. The Question of Timescale Associated with the Determination of Molecular Structures. *Polyhedron* **1988**, *7* (24), 2549–2552.
- (64) Chaudhary, K. K.; Mishra, N. A Review on Molecular Docking: Novel Tool for Drug Discovery. *databases* **2016**, *3* (4), 1029.
- (65) Cozzini, P.; Kellogg, G. E.; Spyralis, F.; Abraham, D. J.; Costantino, G.; Emerson, A.; Fanelli, F.; Gohlke, H.; Kuhn, L. A.; Morris, G. M. Target Flexibility: An Emerging Consideration in Drug Discovery and Design. *J Med Chem* **2008**, *51* (20), 6237–6255.
- (66) Chiarparin, E.; Packer, M. J.; Wilson, D. M. Experimental Free Ligand Conformations: A Missing Link in Structure-Based Drug Discovery. *Future Medicinal Chemistry*. Future Science 2019, pp 79–82.
- (67) Fang, Z.; Song, Y.; Zhan, P.; Zhang, Q.; Liu, X. Conformational Restriction: An Effective Tactic in 'follow-on'-Based Drug Discovery. *Future Med Chem* **2014**, *6* (8), 885–901.

- (68) Park, J.; Tai, J.; Roessner, C. A.; Scott, A. I. Enzymatic Synthesis of S-Adenosyl-L-Methionine on the Preparative Scale. *Bioorg Med Chem* **1996**, *4* (12), 2179–2185.
- (69) Matos, J. R.; Raushel, F. M.; Wong, C.-H. S-adenosylmethionine: Studies on Chemical and Enzymatic Synthesis. *Biotechnol Appl Biochem* **1987**, *9* (1), 39–52.
- (70) Mato, J.; Alvarez, L.; Ortiz, P.; Pajares, M. A. S-Adenosylmethionine Synthesis: Molecular Mechanisms and Clinical Implications. *Pharmacol Ther* **1997**, *73* (3), 265–280.
- (71) De La Haba, G.; Jamieson, G. A.; Mudd, S. H.; Richards, H. H. S-Adenosylmethionine: The Relation of Configuration at the Sulfonium Center to Enzymatic Reactivity<sup>1</sup>. *J Am Chem Soc* **1959**, *81* (15), 3975–3980.
- (72) Markham, G. D.; DeParasis, J.; Gatmaitan, J. The Sequence of MetK, the Structural Gene for S-Adenosylmethionine Synthetase in Escherichia Coli. *Journal of Biological Chemistry* **1984**, *259* (23), 14505–14507.
- (73) Mato, J.; Alvarez, L.; Ortiz, P.; Pajares, M. A. S-Adenosylmethionine Synthesis: Molecular Mechanisms and Clinical Implications. *Pharmacol Ther* **1997**, *73* (3), 265–280.
- (74) Pang, H.; Lilla, E. A.; Zhang, P.; Zhang, D.; Shields, T. P.; Scott, L. G.; Yang, W.; Yokoyama, K. Mechanism of Rate Acceleration of Radical C–C Bond Formation Reaction by a Radical SAM GTP 3', 8-Cyclase. *J Am Chem Soc* **2020**, *142* (20), 9314–9326.
- (75) Bronkhorst, A. J.; Ungerer, V.; Holdenrieder, S. Comparison of Methods for the Quantification of Cell-Free DNA Isolated from Cell Culture Supernatant. *Tumor Biology* **2019**, *41* (8), 1010428319866369.
- (76) Goldberg, S. Mechanical/Physical Methods of Cell Distribution and Tissue Homogenization. In *Proteomic Profiling*; Springer, 2015; pp 1–20.
- (77) Becker, W.; Scherer, A.; Faust, C.; Bauer, D. K.; Scholtes, S.; Rao, E.; Hofmann, J.; Schauder, R.; Langer, T. A Fully Automated Three-Step Protein Purification Procedure for up to Five Samples Using the NGC Chromatography System. *Protein Expr Purif* **2019**, *153*, 1–6.
- (78) Pang, H.; Lilla, E. A.; Zhang, P.; Zhang, D.; Shields, T. P.; Scott, L. G.; Yang, W.; Yokoyama, K. Mechanism of Rate Acceleration of Radical C–C Bond Formation Reaction by a Radical SAM GTP 3',8-Cyclase. *J Am Chem Soc* **2020**, *142* (20), 9314–9326.  
<https://doi.org/10.1021/jacs.0c01200>.
- (79) Schlesier, J.; Siegrist, J.; Gerhardt, S.; Erb, A.; Blaesi, S.; Richter, M.; Einsle, O.; Andexer, J. N. Structural and Functional Characterisation of the Methionine Adenosyltransferase from Thermococcus Kodakarensis. *BMC Struct Biol* **2013**, *13* (1), 1–10.
- (80) Kiefer, J.; Stärk, A.; Kiefer, A. L.; Glade, H. Infrared Spectroscopic Analysis of the Inorganic Deposits from Water in Domestic and Technical Heat Exchangers. *Energies (Basel)* **2018**, *11* (4), 798.
- (81) Chase Jr, M. W.; Tables, N.-J. T. Data Reported in NIST Standard Reference Database 69, June 2005 Release: NIST Chemistry WebBook. *J. Phys. Chem. Ref. Data, Monograph* **1998**, *9*, 1–1951.

- (82) Park, J.; Tai, J.; Roessner, C. A.; Scott, A. I. Overcoming Product Inhibition of S-Adenosyl-L-Methionine (SAM) Synthetase: Preparation of SAM on the 30 MM Scale. *Bioorg Med Chem Lett* **1995**, *5* (19), 2203–2206.
- (83) Oroz-Guinea, I.; García-Junceda, E. Enzyme Catalysed Tandem Reactions. *Curr Opin Chem Biol* **2013**, *17* (2), 236–249.
- (84) Heinonen, J. K. *Biological Role of Inorganic Pyrophosphate*; Springer Science & Business Media, 2001.
- (85) Iwig, D. F.; Booker, S. J. Insight into the Polar Reactivity of the Onium Chalcogen Analogues of S-Adenosyl-L-Methionine. *Biochemistry* **2004**, *43* (42), 13496–13509.
- (86) Matos, J. R.; Wong, C.-H. S-Adenosylmethionine: Stability and Stabilization. *Bioorg Chem* **1987**, *15* (1), 71–80.
- (87) Desiderio, C.; Cavallaro, R. A.; De Rossi, A.; D'Anselmi, F.; Fuso, A.; Scarpa, S. Evaluation of Chemical and Diastereoisomeric Stability of S-Adenosylmethionine in Aqueous Solution by Capillary Electrophoresis. *J Pharm Biomed Anal* **2005**, *38* (3), 449–456.
- (88) Lankau, T.; Kuo, T. N.; Yu, C. H. Computational Study of the Degradation of S-Adenosyl Methionine in Water. *J Phys Chem A* **2017**, *121* (2), 505–514.
- (89) Matos, J. R.; Wong, C.-H. S-Adenosylmethionine: Stability and Stabilization. *Bioorg Chem* **1987**, *15* (1), 71–80.
- (90) Stolowitz, M. L.; Minch, M. J. S-Adenosyl-L-Methionine and S-Adenosyl-L-Homocysteine, an NMR Study. *J Am Chem Soc* **1981**, *103* (20), 6015–6019.
- (91) Nart, F. C.; Iwasita, T.; Weber, M. Sulfate Adsorption on Well-Defined Pt (100) Electrodes. *Electrochim Acta* **1994**, *39* (13), 2093–2096.
- (92) Coblenz Society, Inc. *Sodium sulfate*. National Institute of Standard Reference Database, U.S. Department of commerce.
- (93) Lin, C.-K.; Kuo, J.-L. Anharmonic IR Spectra of Solvated Ammonium and Aminium Ions: Resemblance between Water and Bisulfate Solvations. *Physical Chemistry Chemical Physics* **2022**, *24* (34), 20318–20325.
- (94) Max, J.-J.; Chapados, C. Aqueous Ammonia and Ammonium Chloride Hydrates: Principal Infrared Spectra. *J Mol Struct* **2013**, *1046*, 124–135.
- (95) Smith, A. L. The Coblenz Society Desk Book of Infrared Spectra. *The Coblenz society desk book of infrared spectra* **1982**, *2*.
- (96) Wei, X.-N.; Cao, M.-J.; Li, J.; Li, H.; Song, Y.; Du, C.-H. Synthesis of S-Adenosyl-L-Methionine in Escherichia Coli. *Biotechnology and bioprocess engineering* **2014**, *19*, 958–964.
- (97) Ng, L. M.; Simmons, R. Infrared Spectroscopy. *Anal Chem* **1999**, *71* (12), 343–350.
- (98) Berthomieu, C.; Hienerwadel, R. Fourier Transform Infrared (FTIR) Spectroscopy. *Photosynth Res* **2009**, *101*, 157–170.
- (99) Kötting, C.; Gerwert, K. Proteins in Action Monitored by Time-resolved FTIR Spectroscopy. *ChemPhysChem* **2005**, *6* (5), 881–888.

Preprint not peer reviewed